A New Discontinuous Galerkin Finite Element Method for Directly Solving the Hamilton-Jacobi Equations*

Yingda Cheng [†]   Zixuan Wang [‡]

July 10, 2018

Abstract

In this paper, we improve upon the discontinuous Galerkin (DG) method for Hamilton-Jacobi (HJ) equation with convex Hamiltonians in [5] and develop a new DG method for directly solving the general HJ equations. The new method avoids the reconstruction of the solution across elements by utilizing the Roe speed at the cell interface. Besides, we propose an entropy fix by adding penalty terms proportional to the jump of the normal derivative of the numerical solution. The particular form of the entropy fix was inspired by the Harten and Hyman's entropy fix [12] for Roe scheme for the conservation laws. The resulting scheme is compact, simple to implement even on unstructured meshes, and is demonstrated to work for nonconvex Hamiltonians. Benchmark numerical experiments in one dimension and two dimensions are provided to validate the performance of the method.

Keywords: Hamilton-Jacobi equation, discontinuous Galerkin methods, entropy fix, unstructured mesh.

1   Introduction

In this paper, we consider the numerical solution of the time-dependent Hamilton-Jacobi (HJ) equation

$$\varphi_t + H(\nabla_{\mathbf{x}}\varphi, \mathbf{x}) = 0, \quad \varphi(\mathbf{x}, 0) = \varphi^0(\mathbf{x}), \quad \mathbf{x} \in \Omega \in \mathbb{R}^d \tag{1.1}$$

with suitable boundary conditions on $\partial\Omega$. The HJ equation arises in many applications, e.g., optimal control, differential games, crystal growth, image processing and calculus of variations. The solution of such equation may develop discontinuous derivatives in finite time even when the initial data is smooth. The viscosity solution [8, 7] was introduced as the unique physically relevant solution, and has been the focus of many numerical methods.

†Department of Mathematics, Michigan State University, East Lansing, MI 48824 U.S.A. ycheng@math.msu.edu

‡Department of Mathematics, Michigan State University, East Lansing, MI 48824 U.S.A. wangzix1@msu.edu

Starting from [9, 24], finite difference methods such as essentially non-oscillatory (ENO) [19, 20] or weighted ENO (WENO) methods [14, 27] have been developed to solve the HJ equation. Those finite difference methods work quite efficiently for Cartesian meshes, however they lose the advantage of simplicity on unstructured meshes [1, 27].

Alternatively, the Runge-Kutta discontinuous Galerkin (RKDG) method, originally devised to solve the conservation laws [6], is more flexible for arbitrarily unstructured meshes. The first work of DG methods for HJ equations [13, 17] relies on solving the conservation law system satisfied by the derivatives of the solution. The methods work well numerically even on unstructured mesh, with provable stability results for certain special cases, and were later generalized in eg. [11, 4]. Unfortunately, the procedure of recovering φ from its derivatives has made the algorithm indirect and complicated. In contrast, the design of DG methods for directly solving the HJ equations is appealing but challenging, because the HJ equation is not written in the conservative form, for which the framework of DG methods could easily apply. In [5], a DG method for directly solving the HJ equation was developed. This scheme has provable stability and error estimates for linear equations and demonstrates good convergence to the viscosity solutions for nonlinear equations. However, in entropy violating cells, a correction based on the schemes in [13, 17] is necessary to guarantee stability of the method, and moreover, the method in [5] only works for equations with convex Hamiltonians. Later, this algorithm was applied to solve front propagation problems [3] and front propagation with obstacles [2], in which simplified implementations of the entropy fix procedure were proposed. Meanwhile, central DG [18] and local DG [26] methods were recently developed for the HJ equation. Numerical experiments demonstrate that both methods work for nonconvex Hamiltonians. In addition, the first order version of the local DG method [26] reduces to the monotone schemes and thus has provable convergence properties. However, the central DG methods based on overlapping meshes are difficult to implement on unstructured meshes, and the local DG methods still need to resort to the information about the derivatives of φ, making the method less direct in computation. L^2 error estimates for smooth solutions of the DG method [5] and local DG method [26] have been established in [25]. For recent developments of high order and DG methods for HJ equations, one can refer to the review papers [22, 21].

In this paper, we improve upon the DG scheme in [5] and develop a new DG method for directly solving the general HJ equation. Based on the observation that the method in [5] is closely related to Roe's linearization, we use interfacial terms involving the Roe speed and develop a new entropy fix that was inspired by the Harten and Hyman's entropy fix [12] for Roe scheme for the conservation laws. The new method has the following advantages. Firstly, the scheme is shown to work on unstructured meshes even for nonconvex Hamiltonian. Secondly, the method is simple to implement. The cumbersome L^2 reconstruction of the solutions' derivative at the cell interface in [5] is avoided, and the entropy fix is automatically incorporated by the added jump terms in the derivatives of the numerical solution. Finally, the scheme is direct and compact, and the computation only needs the information about the current cell and its immediate neighbors.

The rest of the paper is organized as follows: in Section 2, we introduce the numerical schemes for one-dimensional and multi-dimensional HJ equations. Section 3 is devoted to the discussion of the numerical results. We conclude and discuss about future work in Section 4.

2 Numerical Methods

In this section, we will describe the numerical methods. We follow the method of lines approach, and below we will only describe the semi-discrete DG schemes. The resulting method of lines ODEs can be solved by the total variation diminishing (TVD) Runge-Kutta methods [23] or strong stability preserving Runge-Kutta methods [10].

2.1 Scheme in one dimension

In this subsection, we will start by designing the scheme for one-dimensional HJ equation. In this case, (1.1) becomes

$$\varphi_t + H(\varphi_x, x) = 0, \qquad \varphi(x, 0) = \varphi^0(x). \tag{2.2}$$

Assume the computational domain is $[a, b]$, we will divide it into N cells as follows

$$a = x_{\frac{1}{2}} < x_{\frac{3}{2}} < \ldots < x_{N+\frac{1}{2}} = b. \tag{2.3}$$

Now the cells and their centers are defined as

$$I_j = (x_{j-\frac{1}{2}}, x_{j+\frac{1}{2}}), \qquad x_j = \frac{1}{2}\left(x_{j-\frac{1}{2}} + x_{j+\frac{1}{2}}\right), \quad j = 1, \cdots, N \tag{2.4}$$

and the mesh sizes are

$$\Delta x_j = x_{j+\frac{1}{2}} - x_{j-\frac{1}{2}}, \qquad h = \max_j \Delta x_j. \tag{2.5}$$

The DG approximation space is

$$V_h^k = \{v : v|_{I_j} \in P^k(I_j), \ j = 1, \cdots, N\} \tag{2.6}$$

where $P^k(I_j)$ denotes all polynomials of degree at most k on I_j, and we let $H_1 = \frac{\partial H}{\partial \varphi_x}$ be the partial derivative of the Hamiltonian with respect to φ_x.

To introduce the scheme, we need to define several quantities at the cell interface where the DG solution is discontinuous. If x_* is a point located at the cell interface, then $\varphi_h \in V_h^k$ would be discontinuous at x_*. We can then define the Roe speed at x_* to be

$$\tilde{H}_{\varphi_h}(x_*) := \begin{cases} \frac{H((\varphi_h)_x(x_*^+), x_*^+) - H((\varphi_h)_x(x_*^-), x_*^-)}{(\varphi_h)_x(x_*^+) - (\varphi_h)_x(x_*^-)}, & \text{if } (\varphi_h)_x(x_*^+) \neq (\varphi_h)_x(x_*^-) \\ \frac{1}{2}(H_1((\varphi_h)_x(x_*^+), x_*^+) + H_1((\varphi_h)_x(x_*^-), x_*^-)), & \text{if } (\varphi_h)_x(x_*^+) = (\varphi_h)_x(x_*^-). \end{cases}$$

In the notations above, we use superscripts $+, -$ to denote the right, and left limits of a function. Notice that in order for the above definition to make sense, we restrict our attention to $k \geq 1$ case, i.e. piecewise linear polynomials and above.

Similar to Harten and Hyman's entropy fix [12], to detect entropy violating cell, we introduce

$$\delta_{\varphi_h}(x_*) := \max\left(0, \tilde{H}_{\varphi_h}(x_*) - H_1((\varphi_h)_x(x_*^-), x_*^-), H_1((\varphi_h)_x(x_*^+), x_*^+) - \tilde{H}_{\varphi_h}(x_*)\right)$$

and

$$S_{\varphi_h}(x_*) := \max\left(\delta_{\varphi_h}(x_*), |\tilde{H}_{\varphi_h}(x_*)|\right).$$

3

We can see that $S_{\varphi_h}(x_*) \neq |\tilde{H}_{\varphi_h}(x_*)|$ only if $|\tilde{H}_{\varphi_h}(x_*)| < \delta_{\varphi_h}(x_*)$.

Now we are ready to formulate our DG scheme for (2.2). We look for $\varphi_h(x,t) \in V_h^k$, such that

$$
\int_{I_j} (\partial_t \varphi_h(x,t) + H(\partial_x \varphi_h(x,t), x)) v_h(x)\, dx
$$
$$
+ \min\left(\tilde{H}_{\varphi_h}(x_{j+\frac{1}{2}}), 0\right) [\varphi_h]_{j+\frac{1}{2}} (v_h)_{j+\frac{1}{2}}^- + \max\left(\tilde{H}_{\varphi_h}(x_{j-\frac{1}{2}}), 0\right) [\varphi_h]_{j-\frac{1}{2}} (v_h)_{j-\frac{1}{2}}^+
$$
$$
- C\Delta x_j (S_{\varphi_h}(x_{j+\frac{1}{2}}) - |\tilde{H}_{\varphi_h}(x_{j+\frac{1}{2}})|)[(\varphi_h)_x]_{j+\frac{1}{2}} (v_h)_{j+\frac{1}{2}}^-
$$
$$
- C\Delta x_j (S_{\varphi_h}(x_{j-\frac{1}{2}}) - |\tilde{H}_{\varphi_h}(x_{j-\frac{1}{2}})|)[(\varphi_h)_x]_{j-\frac{1}{2}} (v_h)_{j-\frac{1}{2}}^+
$$
$$
= 0, \qquad \forall j = 1, \ldots, N \tag{2.7}
$$

holds for any $v_h \in V_h^k$ with $k \geq 1$. Here $[u] = u^+ - u^-$ denotes the jump of a function at the cell interface, Δx_j serves as the scaling factor. C is a positive penalty parameter. The detailed discussion about the choice of C is contained in Section 3. In particular, we find that $C = 0.25$ works well in practice.

Next, we provide interpretation of the scheme (2.7) for the linear HJ equation with variable coefficient

$$
\varphi_t + a(x)\varphi_x = 0
$$

to illustrate the main ideas. Firstly, if $a(x) \in C^1$, then

$$
\tilde{H}_{\varphi_h}(x_{j+\frac{1}{2}}) = a(x_{j+\frac{1}{2}}), \ \delta_{\varphi_h}(x_{j+\frac{1}{2}}) = 0, \ S_{\varphi_h}(x_{j+\frac{1}{2}}) = |a(x_{j+\frac{1}{2}})| \quad \forall j = 1, \ldots, N,
$$

therefore scheme (2.7) reduces to

$$
\int_{I_j} (\partial_t \varphi_h(x,t) + a(x)\partial_x \varphi_h(x,t)) v_h(x)\, dx
$$
$$
+ \min\left(a(x_{j+\frac{1}{2}}), 0\right) [\varphi_h]_{j+\frac{1}{2}} (v_h)_{j+\frac{1}{2}}^- + \max\left(a(x_{j-\frac{1}{2}}), 0\right) [\varphi_h]_{j-\frac{1}{2}} (v_h)_{j-\frac{1}{2}}^+ = 0, \quad j = 1, \ldots, N. \tag{2.8}
$$

This is the same DG method as in [5], and it is the standard DG schemes for the conservation laws with source term

$$
\varphi_t + (a(x)\varphi)_x = a_x(x)\varphi
$$

with Roe flux. Therefore, stability and error estimates could be established [5].

On the other hand, when $a(x)$ is no longer smooth, especially when $a(x)$ contains discontinuity at cell interfaces. The scheme (2.8) will produce entropy violating shocks in the solutions' derivative [5]. In this case, the penalty terms in (2.7) come into play, and the added viscosity enables us to capture the viscosity solution as demonstrated in Section 3. In particular, suppose $a(x)$ is discontinuous at $x_{j+\frac{1}{2}}$, then

$$
\tilde{H}_{\varphi_h}(x_{j+\frac{1}{2}}) = \frac{[a(x)\varphi_h]_{j+\frac{1}{2}}}{[\varphi_h]_{j+\frac{1}{2}}}.
$$

4

If the entropy condition is violated at $x_{j+\frac{1}{2}}$, i.e. $a(x_{j+\frac{1}{2}}^-) < 0 < a(x_{j+\frac{1}{2}}^+)$, then

$$\delta_{\varphi_h}(x_{j+\frac{1}{2}}) = \max\left(0, \frac{[a(x)\varphi_h]_{j+\frac{1}{2}}}{[\varphi_h]_{j+\frac{1}{2}}} - a(x_{j+\frac{1}{2}}^-), a(x_{j+\frac{1}{2}}^+) - \frac{[a(x)\varphi_h]_{j+\frac{1}{2}}}{[\varphi_h]_{j+\frac{1}{2}}}\right) > 0,$$

and $S_{\varphi_h}(x_{j+\frac{1}{2}}) > 0$. When $|\tilde{H}_{\varphi_h}(x_{j+\frac{1}{2}})| < \delta_{\varphi_h}(x_{j+\frac{1}{2}})$, the penalty term

$$-C\Delta x_j (S_{\varphi_h}(x_{j+\frac{1}{2}}) - |\tilde{H}_{\varphi_h}(x_{j+\frac{1}{2}})|)[(\varphi_h)_x]_{j+\frac{1}{2}}(v_h)_{j+\frac{1}{2}}^-$$

will be nonzero. On the other hand, if $a(x_{j+\frac{1}{2}}^-) > 0 > a(x_{j+\frac{1}{2}}^+)$, corresponding to a shock in φ_x, we know the Roe scheme (2.8) could correctly capture this behavior. In fact, in this case

$$\delta_{\varphi_h}(x_{j+\frac{1}{2}}) = \max\left(0, \frac{[a(x)\varphi_h]_{j+\frac{1}{2}}}{[\varphi_h]_{j+\frac{1}{2}}} - a(x_{j+\frac{1}{2}}^-), a(x_{j+\frac{1}{2}}^+) - \frac{[a(x)\varphi_h]_{j+\frac{1}{2}}}{[\varphi_h]_{j+\frac{1}{2}}}\right) = 0,$$

and $S_{\varphi_h}(x_{j+\frac{1}{2}}) - |\tilde{H}_{\varphi_h}(x_{j+\frac{1}{2}})| = 0$, the method (2.7) will reduce to (2.8). Similar arguments extend to the nonlinear case for sonic expanding cells for convex Hamiltonians,

$$H_1(\varphi_x^-(x_{j+\frac{1}{2}})) < 0 < H_1(\varphi_x^+(x_{j+\frac{1}{2}})).$$

The penalty term in (2.7) would be turned on automatically.

Finally we remark that the key differences of the scheme (2.7) compared to the method in [5] are: (1) the L^2 reconstruction of φ_h across two elements is avoided, and we use the Roe speed which could be easily computed. This is advantageous especially for multi-dimensional problems on unstructured meshes, as illustrated in Sections 2.2 and 2.3. (2) The added penalty terms automatically treat the sonic points, and the key idea is to add the viscosity based on the jump in $(\varphi_h)_x$, but not φ_h itself. This is natural considering the formation of monotone schemes such as the Lax-Friedrichs scheme for HJ equation. We will verify in Section 3 that the penalty terms do not degrade the order of the accuracy of the numerical scheme.

2.2   Scheme on two-dimensional Cartesian meshes

In this subsection, we generalize the scheme to compute on two-dimensional Cartesian meshes. Now equation (1.1) is written as

$$\varphi_t + H(\varphi_x, \varphi_y, x, y) = 0, \quad \varphi(x, y, 0) = \varphi^0(x, y), \quad (x, y) \in [a, b] \times [c, d]. \tag{2.9}$$

The rectangular mesh is defined by

$$a = x_{\frac{1}{2}} < x_{\frac{3}{2}} < \ldots < x_{N_x+\frac{1}{2}} = b, \qquad c = y_{\frac{1}{2}} < y_{\frac{3}{2}} < \ldots < y_{N_y+\frac{1}{2}} = d \tag{2.10}$$

and

$$I_{i,j} = [x_{i-\frac{1}{2}}, x_{i+\frac{1}{2}}] \times [y_{j-\frac{1}{2}}, y_{j+\frac{1}{2}}], \quad J_i = [x_{i-1/2}, x_{i+1/2}], \quad K_j = [y_{j-1/2}, y_{j+1/2}]$$
$$i = 1, \ldots N_x, \quad j = 1, \ldots N_y. \tag{2.11}$$

5

Let

$$\Delta x_i = x_{i+1/2} - x_{i-1/2}, \quad \Delta y_j = y_{j+1/2} - y_{j-1/2}, \quad h = \max(\max_i \Delta x_i, \max_j \Delta y_j).$$

We define the approximation space as

$$V_h^k = \{v : v|_{I_{i,j}} \in P^k(I_{i,j}), \; i = 1, \ldots N_x, \quad j = 1, \ldots N_y\} \tag{2.12}$$

where $P^k(I_{i,j})$ denotes all polynomials of degree at most k on $I_{i,j}$ with $k \geq 1$.

Let us denote $H_1 = \frac{\partial H}{\partial \varphi_x}$ and $H_2 = \frac{\partial H}{\partial \varphi_y}$. Similar to the one-dimensional case, we need to introduce several numerical quantities at the cell interface.

If x_* is located at the cell interface in the x direction, then $\varphi_h \in V_h^k$ is discontinuous at (x_*, y) for any y, and we define the Roe speed in the x direction at (x_*, y) to be

$$\tilde{H}_{1,\varphi_h}(x_*, y) :=$$
$$\begin{cases} \frac{H((\varphi_h)_x(x_*^+,y), \overline{(\varphi_h)_y}, x_*^+, y) - H((\varphi_h)_x(x_*^-,y), \overline{(\varphi_h)_y}, x_*^-, y)}{(\varphi_h)_x(x_*^+,y) - (\varphi_h)_x(x_*^-,y)}, & \text{if } (\varphi_h)_x(x_*^+, y) \neq (\varphi_h)_x(x_*^-, y) \\ \frac{1}{2}(H_1((\varphi_h)_x(x_*^+, y), \overline{(\varphi_h)_y}, x_*^+, y) + H_1((\varphi_h)_x(x_*^-, y), \overline{(\varphi_h)_y}, x_*^-, y)), & \text{if } (\varphi_h)_x(x_*^+, y) = (\varphi_h)_x(x_*^-, y), \end{cases}$$

where

$$\overline{(\varphi_h)_y} = \frac{1}{2}\left((\varphi_h)_y(x_*^+, y) + (\varphi_h)_y(x_*^-, y)\right)$$

is the average of the tangential derivative. Again, we define

$$\delta_{1,\varphi_h}(x_*, y) :=$$
$$\max\left(0, \tilde{H}_{1,\varphi_h}(x_*, y) - H_1((\varphi_h)_x(x_*^-, y), \overline{(\varphi_h)_y}, x_*^-, y), H_1((\varphi_h)_x(x_*^+, y), \overline{(\varphi_h)_y}, x_*^+, y) - \tilde{H}_{1,\varphi_h}(x_*, y)\right)$$

and

$$S_{1,\varphi_h}(x_*, y) := \max\left(\delta_{1,\varphi_h}(x_*, y), |\tilde{H}_{1,\varphi_h}(x_*, y)|\right).$$

Similarly, for y_* located at the cell interface in the y direction, $\varphi_h \in V_h^k$ is discontinuous at (x, y_*) for any x, and we define the Roe speed in the y direction at (x, y_*) to be

$$\tilde{H}_{2,\varphi_h}(x, y_*) :=$$
$$\begin{cases} \frac{H(\overline{(\varphi_h)_x}, (\varphi_h)_y(x,y_*^+), x, y_*^+) - H(\overline{(\varphi_h)_x}, (\varphi_h)_y(x,y_*^-), x, y_*^-)}{(\varphi_h)_y(x,y_*^+) - (\varphi_h)_y(x,y_*^-)}, & \text{if } (\varphi_h)_y(x, y_*^+) \neq (\varphi_h)_y(x, y_*^-) \\ \frac{1}{2}(H_1(\overline{(\varphi_h)_x}, (\varphi_h)_y(x, y_*^+), x, y_*^+) + H_1(\overline{(\varphi_h)_x}, (\varphi_h)_y(x, y_*^-), x, y_*^-)), & \text{if } (\varphi_h)_y(x, y_*^+) = (\varphi_h)_y(x, y_*^-), \end{cases}$$

where

$$\overline{(\varphi_h)_x} = \frac{1}{2}\left((\varphi_h)_x(x, y_*^+) + (\varphi_h)_x(x, y_*^-)\right)$$

is the average of the tangential derivative. Again, we define

$$\delta_{2,\varphi_h}(x, y_*) :=$$
$$\max\left(0, \tilde{H}_{2,\varphi_h}(x, y_*) - H_2(\overline{(\varphi_h)_x}, (\varphi_h)_y(x, y_*^-), x, y_*^-), H_2(\overline{(\varphi_h)_x}, (\varphi_h)_y(x, y_*^+), x, y_*^+) - \tilde{H}_{2,\varphi_h}(x, y_*)\right)$$

and

$$S_{2,\varphi_h}(x, y_*) := \max\left(\delta_{2,\varphi_h}(x, y_*), |\tilde{H}_{2,\varphi_h}(x, y_*)|\right).$$

We now formulate our scheme as: find $\varphi_h(x, t) \in V_h^k$, such that

$$\int_{I_{i,j}} (\partial_t \varphi_h(x, y, t) + H(\partial_x \varphi_h(x, y, t), \partial_y \varphi_h(x, y, t), x, y)) v_h(x, y) dx dy$$

$$+ \int_{K_j} \min\left(\tilde{H}_{1,\varphi_h}(x_{i+\frac{1}{2}}, y), 0\right) [\varphi_h](x_{i+\frac{1}{2}}, y) v_h(x_{i+\frac{1}{2}}^-, y) dy$$

$$+ \int_{K_j} \max\left(\tilde{H}_{1,\varphi_h}(x_{i-\frac{1}{2}}, y), 0\right) [\varphi_h](x_{i-\frac{1}{2}}, y) v_h(x_{i-\frac{1}{2}}^+, y) dy$$

$$+ \int_{J_i} \min\left(\tilde{H}_{2,\varphi_h}(x, y_{j+\frac{1}{2}}), 0\right) [\varphi_h](x, y_{j+\frac{1}{2}}) v_h(x, y_{j+\frac{1}{2}}^-) dx$$

$$+ \int_{J_i} \max\left(\tilde{H}_{2,\varphi_h}(x, y_{j-\frac{1}{2}}), 0\right) [\varphi_h](x, y_{j-\frac{1}{2}}) v_h(x, y_{j-\frac{1}{2}}^+) dx \tag{2.13}$$

$$- C\Delta x_i \int_{K_j} \left(S_{1,\varphi_h}(x_{i+\frac{1}{2}}, y) - |\tilde{H}_{1,\varphi_h}(x_{i+\frac{1}{2}}, y)|\right) [(\varphi_h)_x](x_{i+\frac{1}{2}}, y) v_h(x_{i+\frac{1}{2}}^-, y) dy$$

$$- C\Delta x_i \int_{K_j} \left(S_{1,\varphi_h}(x_{i-\frac{1}{2}}, y) - |\tilde{H}_{1,\varphi_h}(x_{i-\frac{1}{2}}, y)|\right) [(\varphi_h)_x](x_{i-\frac{1}{2}}, y) v_h(x_{i-\frac{1}{2}}^+, y) dy$$

$$- C\Delta y_j \int_{J_i} \left(S_{2,\varphi_h}(x, y_{j+\frac{1}{2}}) - |\tilde{H}_{2,\varphi_h}(x, y_{j+\frac{1}{2}})|\right) [(\varphi_h)_y](x, y_{j+\frac{1}{2}}) v_h(x, y_{j+\frac{1}{2}}^-) dx$$

$$- C\Delta y_j \int_{J_i} \left(S_{2,\varphi_h}(x, y_{j-\frac{1}{2}}) - |\tilde{H}_{2,\varphi_h}(x, y_{j-\frac{1}{2}})|\right) [(\varphi_h)_y](x, y_{j-\frac{1}{2}}) v_h(x, y_{j-\frac{1}{2}}^+) dx = 0$$

holds for any $v_h \in V_h^k$ with $k \geq 1$. In practice, the volume and line integrals in (2.13) can be evaluated by Gauss quadrature formulas. The main idea in (2.13) is that in the normal direction of the interface, we apply the ideas from the one-dimensional case, but tangential to the interface, we use the average of the tangential derivatives from the two neighboring cells.

2.3   Scheme on general unstructured meshes

In this subsection, we describe the scheme on general unstructured meshes for (1.1). Let $\mathcal{T}_h = \{K\}$ be a partition of Ω, with K being simplices. We define the piecewise polynomial space

$$V_h^k = \left\{ v \in L^2(\Omega) : v|_K \in P^k(K), \forall K \in \mathcal{T}_h \right\},$$

where $P^k(K)$ denotes the set of polynomials of total degree at most k on K with $k \geq 1$. For any element K, and edge in ∂K, we define $\mathbf{n}_K$ to be the outward unit normal to the boundary of K, and $\mathbf{t}_K$ is the unit tangential vector such that $\mathbf{n}_K \cdot \mathbf{t}_K = 0$. In higher dimensions, i.e. $d > 2$, $d-1$ tangential vectors need to be defined. In addition, for any function $u \in V_h^k$, and $\mathbf{x} \in \partial K$, we define the traces of u_h from outside and inside of the element K to be

$$u_h^{\pm}(\mathbf{x}) = \lim_{\epsilon \downarrow 0} u_h(\mathbf{x} \pm \epsilon \mathbf{n}_k),$$

and $[u_h](\mathbf{x}) = u_h^+(\mathbf{x}) - u_h^-(\mathbf{x})$, $\overline{u_h}(\mathbf{x}) = \frac{1}{2}(u_h^+(\mathbf{x}) + u_h^-(\mathbf{x}))$. We also let $H_{\mathbf{n}_K} = \nabla_{\nabla \varphi} H \cdot \mathbf{n}_K$.

Now following the Cartesian case, we define, for any $\mathbf{x} \in \partial K$,

$$\tilde{H}_{\mathbf{n}_K,\varphi_h}(\mathbf{x}) :=$$
$$\begin{cases} \frac{H((\nabla_{\mathbf{x}}\varphi_h \cdot \mathbf{n}_K)^+, \overline{\nabla_{\mathbf{x}}\varphi_h \cdot \mathbf{t}_K}, \mathbf{x}^+) - H((\nabla_{\mathbf{x}}\varphi_h \cdot \mathbf{n}_K)^-, \overline{\nabla_{\mathbf{x}}\varphi_h \cdot \mathbf{t}_K}, \mathbf{x}^-)}{[\nabla_{\mathbf{x}}\varphi_h \cdot \mathbf{n}_K](\mathbf{x})}, & \text{if } [\nabla_{\mathbf{x}}\varphi_h \cdot \mathbf{n}_K](\mathbf{x}) \neq 0 \\ \frac{1}{2}(H_{\mathbf{n}_K}((\nabla_{\mathbf{x}}\varphi_h \cdot \mathbf{n}_K)^+, \overline{\nabla_{\mathbf{x}}\varphi_h \cdot \mathbf{t}_K}, \mathbf{x}^+) + H_{\mathbf{n}_K}((\nabla_{\mathbf{x}}\varphi_h \cdot \mathbf{n}_K)^-, \overline{\nabla_{\mathbf{x}}\varphi_h \cdot \mathbf{t}_K}, \mathbf{x}^-)), & \text{otherwise,} \end{cases}$$

and

$$\delta_{\mathbf{n}_K,\varphi_h}(\mathbf{x}) :=$$
$$\max\left(0, \tilde{H}_{\mathbf{n}_K,\varphi_h}(\mathbf{x}) - H_{\mathbf{n}_K}((\nabla_{\mathbf{x}}\varphi_h \cdot \mathbf{n}_K)^-, \overline{\nabla_{\mathbf{x}}\varphi_h \cdot \mathbf{t}_K}, \mathbf{x}^-), H_{\mathbf{n}_K}((\nabla_{\mathbf{x}}\varphi_h \cdot \mathbf{n}_K)^+, \overline{\nabla_{\mathbf{x}}\varphi_h \cdot \mathbf{t}_K}, \mathbf{x}^+) - \tilde{H}_{\mathbf{n}_K,\varphi_h}(\mathbf{x})\right),$$

$$S_{\mathbf{n}_K,\varphi_h}(\mathbf{x}) := \max\left(\delta_{\mathbf{n}_K,\varphi_h}(\mathbf{x}), |\tilde{H}_{\mathbf{n}_K,\varphi_h}(\mathbf{x})|\right).$$

Then we look for $\varphi_h \in V_h^k$, such that for each K,

$$\int_K ((\varphi_h)_t + H(\nabla_{\mathbf{x}}\varphi_h, \mathbf{x}))\, v_h\, d\mathbf{x} + \int_{\partial K} \min\left(\tilde{H}_{\mathbf{n}_K,\varphi_h}(\mathbf{x}), 0\right) [\varphi_h](\mathbf{x}) v_h^-(\mathbf{x}) ds$$
$$-C\frac{\Delta K}{\Delta S_K} \int_{\partial K} (S_{\mathbf{n}_K,\varphi_h}(\mathbf{x}) - |\tilde{H}_{\mathbf{n}_K,\varphi_h}(\mathbf{x})|)[\nabla_{\mathbf{x}}\varphi_h \cdot \mathbf{n}_K](\mathbf{x}) v_h^-(\mathbf{x}) ds = 0$$

for any test function $v_h \in V_h^k$ with $k \geq 1$, where ΔK, ΔS_K are size of the element K and edge S_K respectively. In practice, the volume and edge integrals need to be evaluated by quadrature rules with enough accuracy. For example, we use quadrature rules that are exact for $(2k)$-th order polynomial for the volume integral, and quadrature rules that are exact for $(2k + 1)$-th order polynomial for the edge integrals.

3   Numerical Results

In this section, we provide numerical results to demonstrate the high order accuracy and reliability of our schemes. In all numerical experiments, we use the third order TVD-RK method as the temporal discretization [23].

3.1   One-dimensional results

In this subsection, we provide computational results for one-dimensional HJ equations.

Example 3.1 We solve the following linear problem with smooth variable coefficient

$$\begin{cases} \varphi_t + \sin(x)\varphi_x = 0 \\ \varphi(x,0) = \sin(x) \\ \varphi(0,t) = \varphi(2\pi,t) \end{cases} \tag{3.14}$$

Since $a(x)$ is smooth in this example, the penalty term automatically vanishes and the choice of C does not have an effect on the solution. We provide the numerical results for P^1, P^2 and P^3 polynomials in Table 3.1. The CFL numbers used are also listed in this table. For P^3 polynomials, we set $\Delta t = O(\Delta x^{\frac{4}{3}})$ in order to get comparable numerical errors in time as in space. From the results, we could clearly observe the optimal $(k+1)$-th order accuracy for P^k polynomials.

Table 3.1: Errors and numerical orders of accuracy for Example 3.1 when using P^k, $k = 1, 2, 3$, polynomials and third order Runge-Kutta time discretization on a uniform mesh of N cells. Final time $t = 1$.

N	L^1 error	order	L^2 error	order	L^∞ error	order
P^1			$CFL = 0.3$			
40	1.20E-03		2.55E-03		1.52E-02	
80	3.07E-04	1.96	6.83E-04	1.90	4.32E-03	1.81
160	7.84E-05	1.97	1.78E-04	1.94	1.14E-03	1.92
320	1.99E-05	1.98	4.56E-05	1.97	2.94E-04	1.96
640	5.03E-06	1.99	1.15E-05	1.98	7.43E-05	1.98
P^2			$CFL = 0.1$			
40	4.76E-05		9.97E-05		5.23E-04	
80	5.97E-06	2.99	1.36E-05	2.88	8.77E-05	2.58
160	7.48E-07	3.00	1.82E-06	2.90	1.35E-05	2.70
320	9.38E-08	2.99	2.38E-07	2.93	1.96E-06	2.78
640	1.18E-08	2.99	3.08E-08	2.95	2.72E-07	2.85
P^3			$CFL = 0.05$			
40	2.12E-06		5.13E-06		2.89E-05	
80	1.36E-07	3.97	3.49E-07	3.89	2.16E-06	3.75
160	8.71E-09	3.97	2.30E-08	3.93	1.57E-07	3.79
320	5.14E-10	4.09	1.35E-09	4.10	9.47E-09	4.06
640	4.83E-12	6.75	9.06E-12	7.24	4.52E-11	7.73
1280	2.03E-13	4.58	2.96E-13	4.94	1.42E-12	5.00

Example 3.2 We solve the following linear problem with nonsmooth variable coefficient [5]

$$\begin{cases} \varphi_t + \text{sign}(\cos(x))\varphi_x = 0 \\ \varphi(x, 0) = \sin(x) \\ \varphi(0, t) = \varphi(2\pi, t) \end{cases} \qquad (3.15)$$

The viscosity solution of this example has a shock forming in φ_x at $x = \pi/2$, and a rarefaction wave at $x = 3\pi/2$. We use this example to demonstrate the effect of the choice of C on the numerical solution. The solutions obtained with different values of C are provided in Figure 3.1. If we take the penalty constant $C = 0$, that is, without entropy correction, the entropy condition is violated at the two cells neighboring $x = 3\pi/2$, and the numerical solution is not convergent towards the exact solution. As we slowly increasing the value of C, we could observe better and better convergence property. In particular, once C passes some threshold, its effect on the quality of the solution is minimum, and bigger values of C only cause slightly larger numerical errors. This is also demonstrated in Table 3.2. For this problem, the viscosity solution is not smooth, so we do not expect the full $(k + 1)$-th order accuracy for this example. However, for different values of C ranging from 0.125 to 1.0, the numerical errors listed in Table 3.2 are all of second order. Actually, for all of the simulations performed in this paper, we find that $C = 0.25$ to be a good choice of the penalty constant. Unless otherwise noted, for the remaining of the paper, we will use $C = 0.25$.
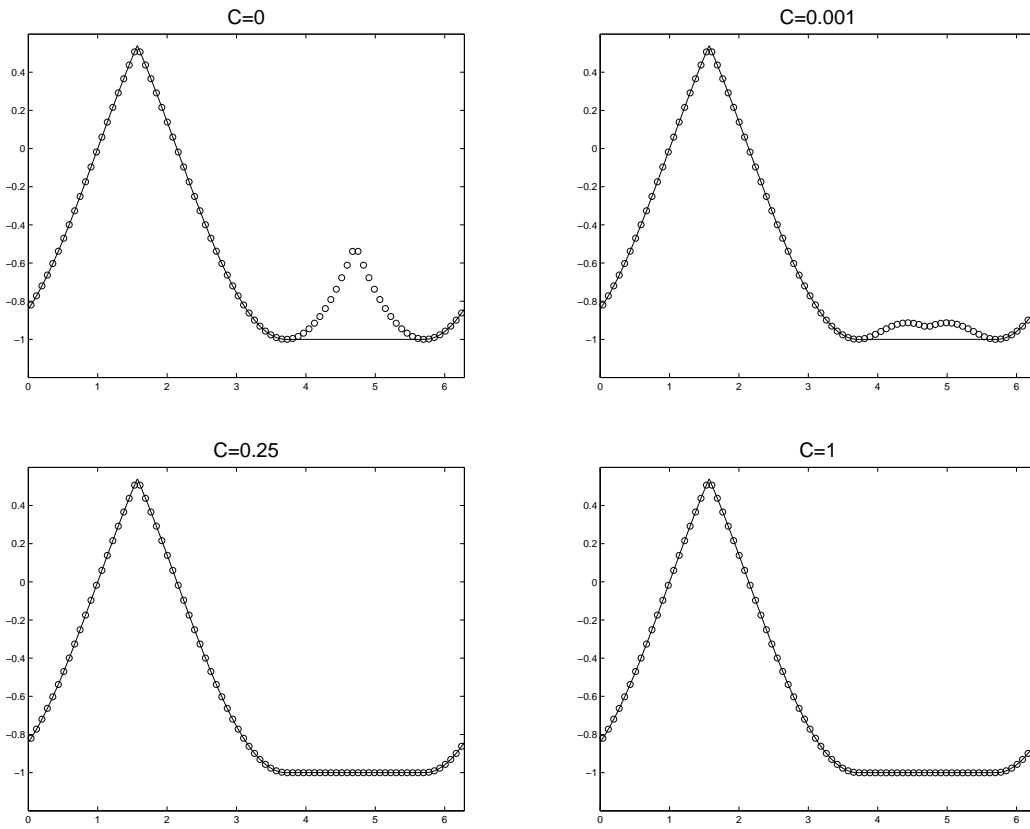
Figure 3.1: Example 3.2. The numerical solution with various values of penalty constant C. $t = 1$. $CFL = 0.1$. P^2 polynomials. $N = 80$. Solid line: the exact solution; circles: the numerical solution.

Table 3.2: Errors and numerical orders of accuracy for Example 3.2 when using P^2 polynomials and third order Runge-Kutta time discretization on a uniform mesh of N cells. Final time $t = 1$. $CFL = 0.1$.

N	L^1 error	order	L^2 error	order	L^∞ error	order
			$C = 1.0$			
40	1.05E-03		1.85E-03		3.49E-03	
80	2.71E-04	1.95	4.78E-04	1.95	8.73E-04	2.00
160	6.89E-05	1.98	1.21E-04	1.98	2.18E-04	2.00
320	1.73E-05	1.99	3.06E-05	1.98	5.46E-05	2.00
640	4.34E-06	2.00	7.67E-06	2.00	1.37E-05	2.00
			$C = 0.5$			
40	9.92E-04		1.74E-03		3.28E-03	
80	2.56E-04	1.95	4.50E-04	1.95	8.22E-04	2.00
160	6.49E-05	1.98	1.14E-04	1.98	2.06E-04	2.00
320	1.63E-05	1.99	2.88E-05	1.98	5.14E-05	2.00
640	4.09E-06	2.00	7.22E-06	2.00	1.29E-05	2.00
			$C = 0.25$			
40	8.74E-04		1.53E-03		2.87E-03	
80	2.25E-04	1.96	3.95E-04	1.95	7.19E-04	2.00
160	5.69E-05	1.98	1.00E-04	1.98	1.80E-04	2.00
320	1.43E-05	1.99	2.52E-05	1.99	4.50E-05	2.00
640	3.58E-06	2.00	6.32E-06	1.99	1.13E-05	2.00
			$C = 0.125$			
40	6.38E-04		1.10E-03		2.05E-03	
80	1.62E-04	1.97	2.84E-04	1.96	5.14E-04	2.00
160	4.09E-05	1.98	7.18E-05	1.98	1.29E-04	2.00
320	1.03E-05	1.99	1.81E-05	1.99	3.23E-05	2.00
640	2.57E-06	2.00	4.53E-06	2.00	8.57E-06	1.91

.

Example 3.3 One-dimensional Burgers' equation with smooth initial condition

$$\begin{cases} \varphi_t + \frac{1}{2}\varphi_x^2 = 0 \\ \varphi(x,0) = \sin(x) \\ \varphi(0,t) = \varphi(2\pi, t) \end{cases} \tag{3.16}$$

At $t = 0.5$, the solution is still smooth, and the optimal $(k+1)$-th accuracy is obtained for P^k polynomials with both uniform and random meshes, see Tables 3.3 and 3.4. At $t = 1$, there will be a shock in φ_x, and our scheme could capture the kink sharply as shown in Figure 3.2.

Example 3.4 One-dimensional Burgers' equation with a nonsmooth initial condition [5]

$$\begin{cases} \varphi_t + \frac{1}{2}\varphi_x^2 = 0 \\ \varphi(x,0) = \begin{cases} \pi - x & \text{if} \quad 0 \leq x \leq \pi \\ x - \pi & \text{if} \quad 0 \leq x \leq 2\pi \end{cases} \\ \varphi(0,t) = \varphi(2\pi, t) \end{cases} \tag{3.17}$$

Table 3.3: Errors and numerical orders of accuracy for Example 3.3 when using P^2 polynomials and third order Runge-Kutta time discretization on a uniform mesh of N cells. Penalty constant $C = 0.25$. Final time $t = 0.5$. $CFL = 0.1$.

| N	L^1 error	order	L^2 error	order	L^∞ error	order
			P^1			
40	8.45E-04		1.23E-03		5.04E-03	
80	2.02E-04	2.07	2.99E-04	2.04	1.27E-03	1.99
160	4.93E-05	2.03	7.42E-05	2.01	3.42E-04	1.89
320	1.22E-05	2.01	1.86E-05	2.00	9.08E-05	1.91
640	3.04E-06	2.01	4.66E-06	2.00	2.36E-05	1.94
			P^2			
40	1.27E-05		2.33E-05		1.28E-04	
80	1.53E-06	3.05	2.93E-06	2.99	2.10E-05	2.61
160	1.91E-07	3.00	3.73E-07	2.98	2.52E-06	3.06
320	2.39E-08	3.00	4.74E-08	2.98	3.56E-07	2.82
640	3.63E-09	2.72	6.23E-09	2.93	4.82E-08	2.88
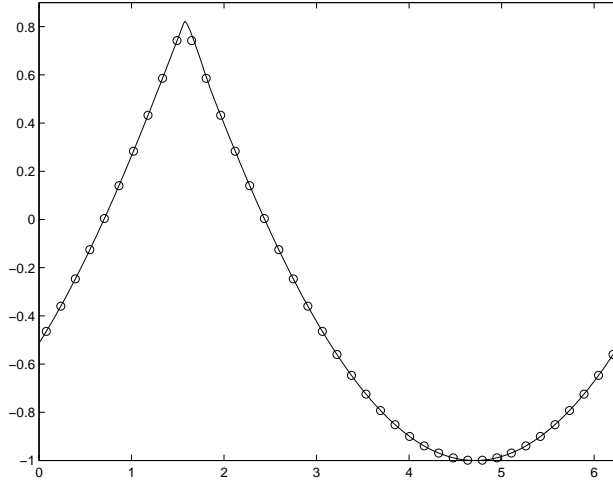
Figure 3.2: Example 3.3. $t = 1.5$. $CFL = 0.1$. P^2 polynomials. $N = 40$. Penalty constant $C = 0.25$. Solid line: the exact solution; circles: the numerical solution.

The exact solution should have a rarefaction wave forming in its derivative, so the initial sharp corner at $x = \pi$ should be smeared out at later times. Since the entropy condition is violated by the Roe type scheme, the entropy fix is necessary for convergence. Figure 3.3 shows the comparison of our schemes with various values of penalty constant C for this nonlinear problem. Again, we could see that $C = 0.25$ is a good choice for this example.

Example 3.5 One-dimensional Eikonal equation

$$\begin{cases} \varphi_t + |\varphi_x| = 0 \\ \varphi(x, 0) = \sin(x) \\ \varphi(0, t) = \varphi(2\pi, t) \end{cases} \tag{3.18}$$
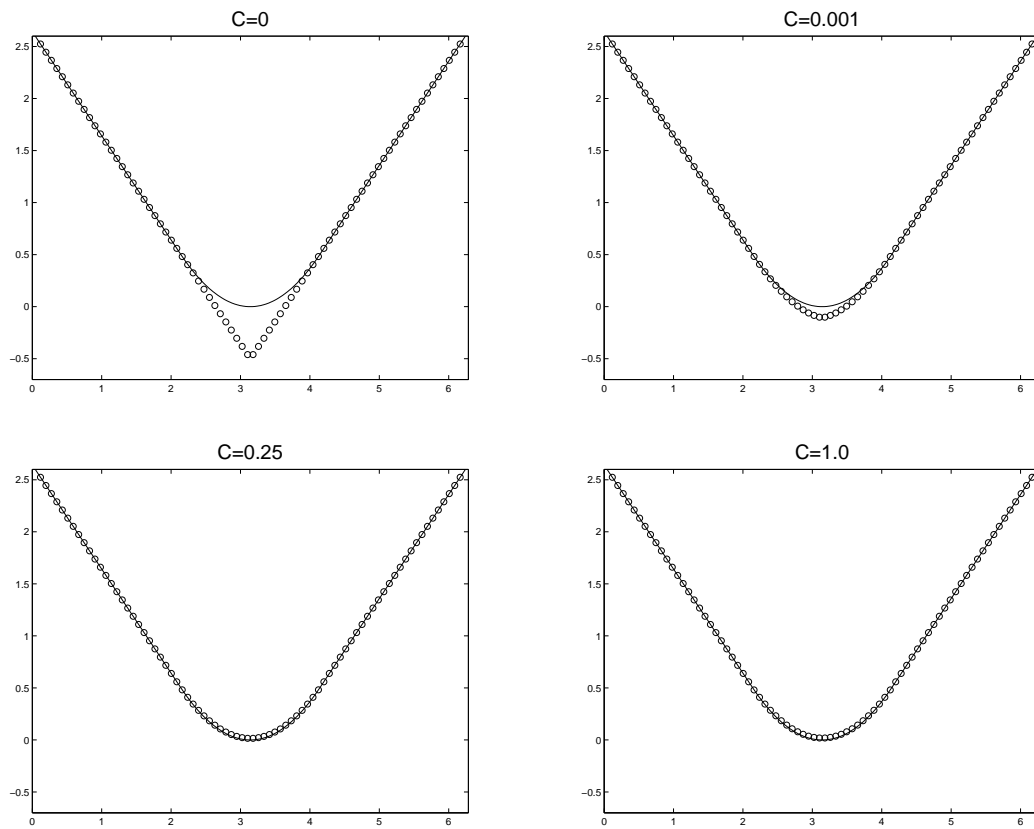
Figure 3.3: Example 3.4. The numerical solution with various values of penalty constant C. $t = 1$. $CFL = 0.1$. P^2 polynomials. $N = 80$. Solid line: the exact solution; circles: the numerical solution.

Table 3.4: Errors and numerical orders of accuracy for Example 3.3 when using P^1 and P^2 polynomials and third order Runge-Kutta time discretization on a random mesh with 40% perturbation of N cells. Penalty constant $C = 0.25$. Final time $t = 0.5$. $CFL = 0.1$.

N	L^1 error	order	L^2 error	order	L^∞ error	order
			P^1			
40	1.23E-03		1.91E-03		1.01E-02	
80	2.70E-04	2.19	4.25E-04	2.17	2.59E-03	1.96
160	6.70E-05	2.01	1.05E-04	2.01	6.22E-04	2.06
320	1.62E-05	2.05	2.67E-05	1.97	2.03E-04	1.61
640	3.97E-06	2.03	6.69E-06	2.00	6.52E-05	1.64
			P^2			
40	2.27E-05		4.52E-05		2.96E-04	
80	2.54E-06	3.16	5.84E-06	2.95	5.25E-05	2.50
160	3.19E-07	3.00	6.87E-07	3.09	5.82E-06	3.17
320	4.00E-08	3.00	9.34E-08	2.88	8.96E-07	2.70
640	5.38E-09	2.89	1.16E-08	3.01	1.32E-07	2.77

The exact solution is the same as the exact solution of Example 3.2. Our scheme could capture the viscosity solution of this nonsmooth Hamiltonian. The numerical errors and orders of accuracy using P^2 polynomials are listed in Table 3.5. Since the solution is not smooth, we do not expect the optimal $(k+1)$-th order accuracy for P^k polynomials.

Table 3.5: Errors and numerical orders of accuracy for Example 3.5 when using P^2 polynomials and third order Runge-Kutta time discretization on a uniform mesh of N cells. Penalty constant $C = 0.25$. Final time $t = 1$. $CFL = 0.1$.

N	L^1 error	order	L^2 error	order	L^∞ error	order
40	6.24E-04		1.09E-03		2.13E-03	
80	1.69E-04	1.88	2.98E-04	1.87	5.54E-04	1.94
160	4.35E-05	1.96	7.67E-05	1.96	1.40E-04	1.98
320	1.10E-05	1.99	1.94E-05	1.99	3.51E-05	2.00
640	2.75E-06	2.00	4.88E-06	1.99	8.77E-06	2.00

Example 3.6 One-dimensional equation with a nonconvex Hamiltonian

$$\begin{cases} \varphi_t - \cos(\varphi_x + 1) = 0 \\ \varphi(x, 0) = -\cos(\pi x) \\ \varphi(-1, t) = \varphi(1, t) \end{cases} \tag{3.19}$$

This example involves a nonconvex Hamiltonian with smooth initial data. At $t = 0.5/\pi^2$, the exact solution is still smooth, and numerical results are presented in Table 3.6, demonstrating the optimal order of accuracy of the scheme. By the time $t = 1.5/\pi^2$, nonsmooth features would develop in φ, which are reliably captured in Figure 3.4.

Example 3.7 One-dimensional Riemann problem with a nonconvex Hamiltonian

$$\begin{cases} \varphi_t + \frac{1}{4}(\varphi_x^2 - 1)(\varphi_x^2 - 4) = 0 \\ \varphi(x, 0) = -2|x| \end{cases} \tag{3.20}$$

Table 3.6: Errors and numerical orders of accuracy for Example 3.6 when using P^2 polynomials and third order Runge-Kutta time discretization on a uniform mesh of N cells. Penalty constants $C = 0.25$. Final time $t = 0.5/\pi^2$. $CFL = 0.1$.

N	L^1 error	order	L^2 error	order	L^∞ error	order
40	1.46E-05		2.16E-05		9.89E-05	
80	1.79E-06	3.02	2.87E-06	2.91	1.59E-05	2.64
160	2.22E-07	3.01	3.73E-07	2.95	2.39E-06	2.74
320	2.76E-08	3.01	4.79E-08	2.96	3.39E-07	2.82
640	3.51E-09	2.98	6.13E-09	2.97	4.53E-08	2.90
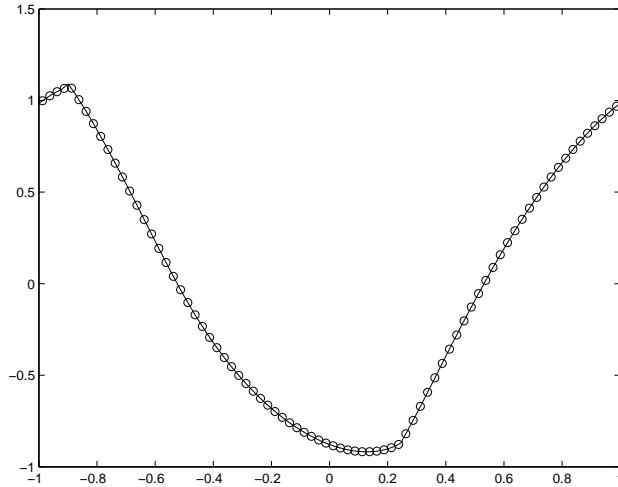
Figure 3.4: Example 3.6. $t = 1.5/\pi^2$. $CFL = 0.1$. P^2 polynomials. $N = 80$. Penalty constant $C = 0.25$. Solid line: the exact solution; circles: the numerical solution.

For this problem, the initial condition has a singularity at $x = 0$. Similar to [18, 26], a nonlinear limiter is needed in order to capture the viscosity solution. We use the standard minmod limiter [6]. This example and Example 3.14 are the only examples needing nonlinear limiting in this paper.

The numerical solutions with and without the limiter are listed in Figure 3.5 for odd and even values of N. Those different behaviors are due to the fact that the singular point $x = 0$ would be exactly located at the cell interface for even N but not odd N at $t = 0$. We note that the method with limiter can correctly capture the viscosity solution for both even and odd N. The numerical errors and orders of accuracy using P^2 polynomials with limiters are listed in Table 3.7. We could see that both methods converge, while the odd N giving slightly smaller errors. However, similar to [18], the method is only first order accurate for this nonsmooth problem.

3.2 Two-dimensional results

In this subsection, we provide computational results for two-dimensional HJ equations on both Cartesian and unstructured meshes.
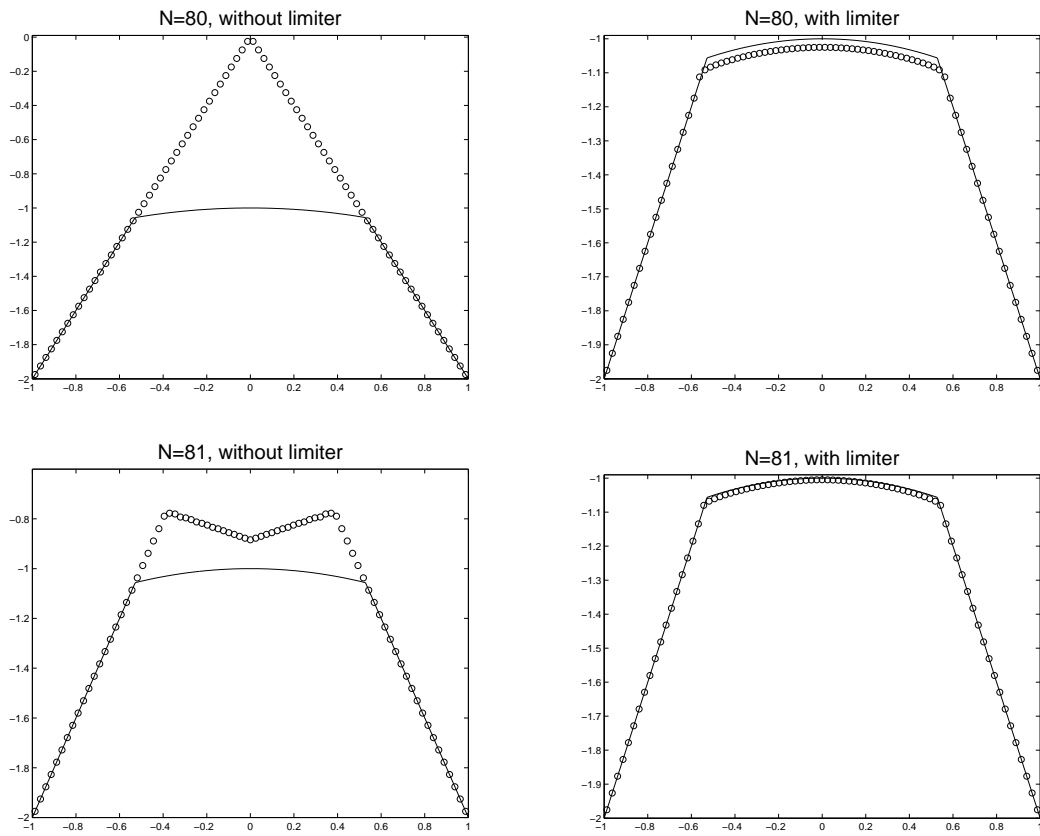
Figure 3.5: Example 3.7. Comparison of the numerical solution with and without the limiter. $t = 1$. P^2 polynomials. $CFL = 0.05$. Penalty constant $C = 0.25$. Left: without limiter; right: with limiter. Solid line: the exact solution; circles: the numerical solution.

Table 3.7: Errors and numerical orders of accuracy for Example 3.7 when using P^2 polynomials and third order Runge-Kutta time discretization on a uniform mesh of N cells. $CFL = 0.05$. Penalty constant $C = 0.25$. Final time $t = 1$. A minmod limiter is used.

N	L^1 error	order	L^2 error	order	L^∞ error	order
			Even N			
40	9.49E-03		2.21E-02		5.96E-02	
80	4.64E-03	1.03	1.10E-02	1.00	3.17E-02	0.91
160	2.28E-03	1.03	5.48E-03	1.00	1.64E-02	0.95
320	1.12E-03	1.02	2.73E-03	1.01	8.40E-03	0.97
640	5.60E-04	1.00	1.36E-03	1.00	4.27E-03	0.98
			Odd N			
41	2.81E-03		6.74E-03		2.94E-02	
81	1.34E-03	1.09	3.35E-03	1.03	2.38E-02	0.31
161	6.41E-04	1.07	1.61E-03	1.06	9.88E-03	1.28
321	3.17E-04	1.02	7.99E-04	1.01	4.36E-03	1.19
641	1.56E-04	1.02	3.96E-04	1.02	3.12E-03	0.49

Example 3.8 Two-dimensional linear problem with smooth variable coefficients

$$\varphi_t - y\varphi_x + x\varphi_y = 0. \tag{3.21}$$

The computational domain is $[-1, 1]^2$. The initial condition is given by

$$\varphi_0(x, y) = \begin{cases} 0 & 0.3 \le r \\ 0.3 - r & 0.1 < r < 0.3 \\ 0.2 & r \le 0.1 \end{cases} \tag{3.22}$$

where $r = \sqrt{(x - 0.4)^2 + (y - 0.4)^2}$. We impose periodic boundary condition on the domain. This is a solid body rotation around the origin. The exact solution can be expressed as

$$\varphi(x, y, t) = \varphi_0(x \cos(t) + y \sin(t), -x \sin(t) + y \cos(t)). \tag{3.23}$$

For this problem, same as the argument in Example 3.1, the choice of C does not have an effect on the scheme. We list the numerical errors and orders in Table 3.8. With this nonsmooth initial condition, we do not expect to obtain $(k + 1)$-th order of accuracy. At $t = 2\pi$, i.e. one period of rotation, we take a snapshot at the line $y = x$ in Figure 3.6. It can be clearly seen that a higher order scheme can yield better results for this nonsmooth initial condition.

Example 3.9 We solve the same equation (3.21) as in Example 3.8, but with a smooth initial condition as

$$\varphi_0(x, y) = \exp\left(-\frac{(x - 0.4)^2 + (y - 0.4)^2}{2\sigma^2}\right). \tag{3.24}$$

The constant $\sigma = 0.05$ is chosen such that at the domain boundary, φ is very small, hence imposing the periodic boundary condition will lead to small errors. We then could observe the optimal order of accuracy in Table 3.9.

Table 3.8: Errors and numerical orders of accuracy for Example 3.8 when using P^2 polynomials and third order Runge-Kutta time discretization on a uniform mesh of $N \times N$ cells. Final time $t = 1$. $CFL = 0.1$.

N	L^1 error	order	L^2 error	order	L^∞ error	order
10	1.21E-03		3.10E-03		2.21E-02	
20	4.13E-04	1.55	1.32E-03	1.23	1.14E-02	0.95
40	1.38E-04	1.58	5.51E-04	1.26	6.49E-03	0.81
80	4.74E-05	1.54	2.36E-04	1.22	3.62E-03	0.84
160	1.54E-05	1.62	1.01E-04	1.23	2.07E-03	0.81
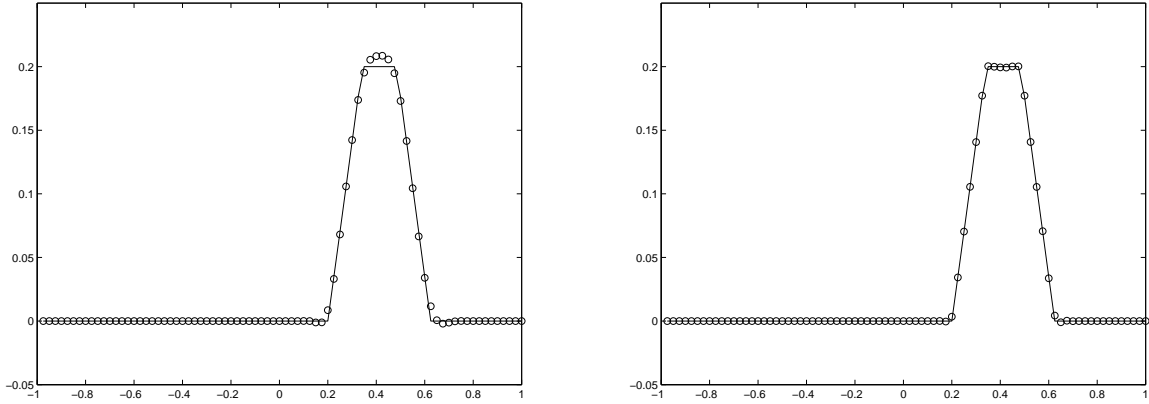
Figure 3.6: Example 3.8. $t = 2\pi$. $CFL = 0.1$. 80×80 uniform mesh. Left: P^1 polynomials; right: P^2 polynomials. One dimensional cut of $45°$ with the x axis. Solid line: the exact solution; circles: the numerical solution.

Example 3.10 Two-dimensional Burgers' equation

$$\begin{cases} \varphi_t + \dfrac{(\varphi_x + \varphi_y + 1)^2}{2} = 0 \\ \varphi(x, y, 0) = -\cos\left(\dfrac{\pi(x+y)}{2}\right) \end{cases} \tag{3.25}$$

with periodic boundary condition on the domain $[-2, 2]^2$.

In this example, we test the performance of our method on unstructured meshes. A sample mesh used with characteristic length $h = 1/4$ is given in Figure 3.7. At $t = 0.5/\pi^2$, the solution is still smooth. Numerical errors and order of accuracy using P^2 polynomials are listed in Table 3.10, demonstrating the optimal order of accuracy. At $t = 1.5/\pi^2$, the solution is no longer smooth. Our scheme could capture the viscosity solution as shown in Figure 3.8.

Example 3.11 Two-dimensional nonlinear equation [18]

$$\begin{cases} \varphi_t + \varphi_x \varphi_y = 0 \\ \varphi(x, y, 0) = \sin(x) + \cos(y) \end{cases} \tag{3.26}$$

with periodic boundary condition on the domain $[-\pi, \pi]^2$.

At $t = 0.8$, the solution is still smooth, as shown in the left figure of Figure 3.9. Numerical errors and order of accuracy using P^2 polynomials are listed in Table 3.11, demonstrating

Table 3.9: Errors and numerical orders of accuracy for Example 3.9 when using P^2 polynomials and third order Runge-Kutta time discretization on a uniform mesh of $N \times N$ cells. Final time $t = 1$. $CFL = 0.1$.

N	L^1 error	order	L^2 error	order	L^∞ error	order
20	1.42E-03		1.03E-02		2.79E-01	
40	1.54E-04	3.20	1.47E-03	2.81	5.25E-02	2.41
80	1.10E-05	3.81	1.10E-04	3.73	5.77E-03	3.19
160	1.12E-06	3.30	1.15E-05	3.26	8.96E-04	2.69
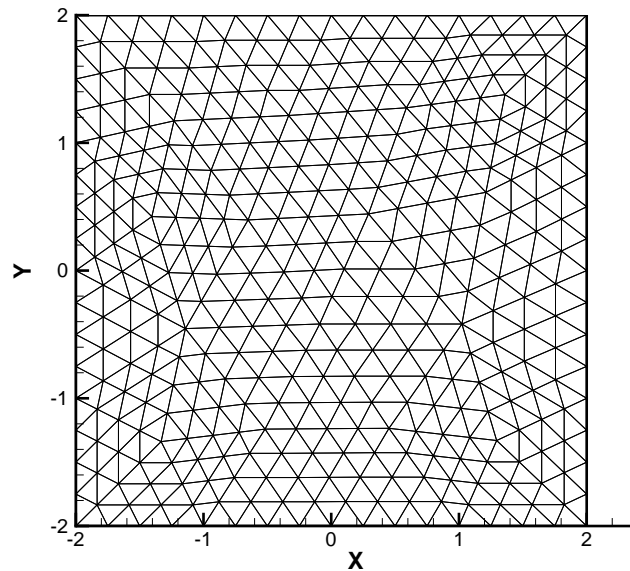
Figure 3.7: Examples 3.10 and 3.13. The unstructured mesh used with characteristic length $h = 1/4$.
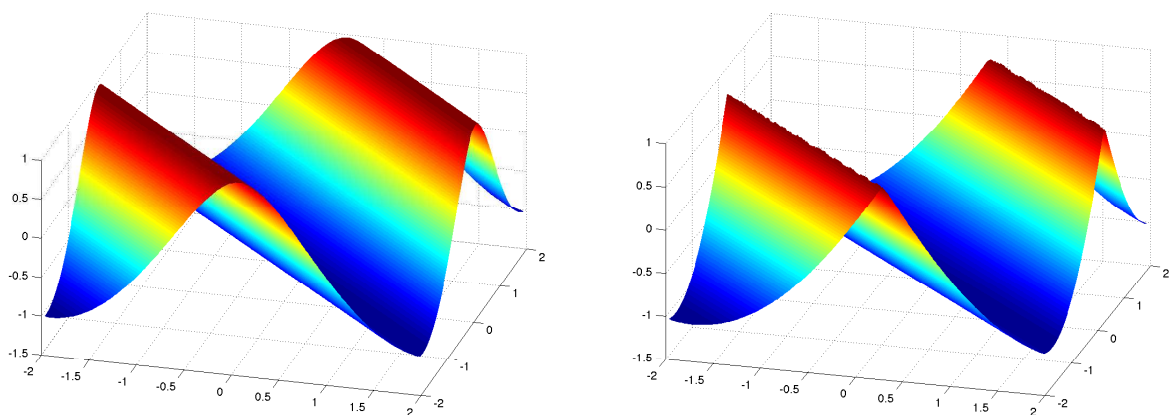
Figure 3.8: Example 3.10. $CFL = 0.1$. P^2 polynomials. Triangular mesh with characteristic length $1/8$. 2816 elements. Penalty constant $C = 0.25$. Left: $t = 0.5/\pi^2$; right: $t = 1.5/\pi^2$.

the optimal order of accuracy. At $t = 1.5$, singular features would form in the solution, as shown in the right figure of Figure 3.9.

19

Table 3.10: Errors and numerical orders of accuracy for Example 3.10 when using P^2 polynomials and third order Runge-Kutta time discretization on triangular meshes with characteristic length h. Penalty constant $C = 0.25$. Final time $t = 0.5/\pi^2$. $CFL = 0.1$.

h	L^1 error	order	L^2 error	order	L^∞ error	order
1	1.36E-02		2.31E-02		2.22E-01	
1/2	1.77E-03	2.93	3.23E-03	2.84	5.14E-02	2.11
1/4	2.25E-04	2.98	4.50E-04	2.84	8.95E-03	2.52
1/8	2.74E-05	3.04	5.82E-05	2.95	1.30E-03	2.78
1/16	3.40E-06	3.01	7.53E-06	2.95	1.84E-04	2.83

Table 3.11: Errors and numerical orders of accuracy for Example 3.11 when using P^2 polynomials and third order Runge-Kutta time discretization on a uniform mesh of $N \times N$ cells. Penalty constant $C = 0.25$. Final time $t = 0.8$. $CFL = 0.1$.

N	L^1 error	order	L^2 error	order	L^∞ error	order
10	2.22E-03		3.95E-03		4.78E-02	
20	2.75E-04	2.98	4.50E-04	2.98	7.79E-03	2.62
40	3.70E-05	2.89	7.33E-05	2.77	1.50E-03	2.38
80	4.80E-06	2.95	9.83E-06	2.90	2.40E-04	2.64

Example 3.12 An example related to controlling optimal cost determination [20]

$$\begin{cases} \varphi_t + \sin(y)\varphi_x + (\sin(x) + \operatorname{sign}(\varphi_y))\varphi_y - \frac{1}{2}\sin^2(y) + \cos(x) - 1 = 0 \\ \varphi(x, y, 0) = 0 \end{cases} \tag{3.27}$$

with periodic boundary condition on the domain $[-\pi, \pi]^2$.

The Hamiltonian is not smooth in this example. Our scheme can capture the features of the viscosity solution well. The numerical solution (left) and the optimal control term $\operatorname{sign}(\varphi_y)$ (right) at $t = 1$ are shown in Figure 3.10.

Example 3.13 Two-dimensional equation with a nonconvex Hamiltonian

$$\begin{cases} \varphi_t - \cos(\varphi_x + \varphi_y + 1) = 0 \\ \varphi(x, y, 0) = -\cos(\frac{\pi}{2}(x + y)) \end{cases} \tag{3.28}$$

with periodic boundary condition on the domain $[-2, 2]^2$.

We use the same unstructured mesh as in Example 3.10, see for example Figure 3.7. At $t = 0.5/\pi^2$, the solution is still smooth, see Table 3.12 for numerical errors and order of accuracy using P^2 polynomials. At $t = 1.5/\pi^2$, singular features would develop in the solution, as shown in Figure 3.11.

Example 3.14 Two-dimensional Riemann problem

$$\begin{cases} \varphi_t + \sin(\varphi_x + \varphi_y) = 0 \\ \varphi(x, y, 0) = \pi(|y| - |x|) \end{cases} \tag{3.29}$$

on the domain $[-1, 1]^2$.

Similar to [13, 26], a nonlinear limiter is needed for convergence in this example. We use the moment limiter [16] and the numerical solution obtained by P^2 polynomial at $t = 1$ is provided in Figure 3.12.
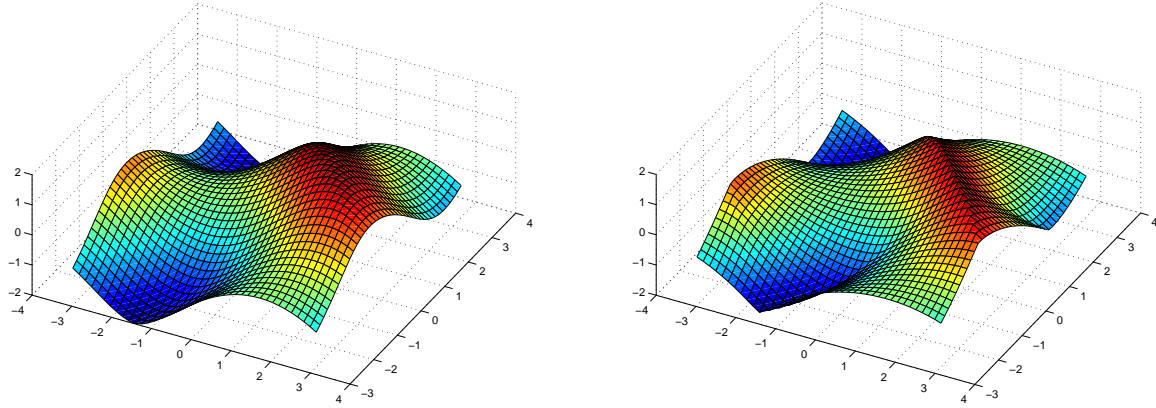
Figure 3.9: Example 3.11. $CFL = 0.1$. P^2 polynomials on a 80×80 uniform mesh. Penalty constant: $C = 0.25$. Left: $t = 0.8$; right: $t = 1.5$.
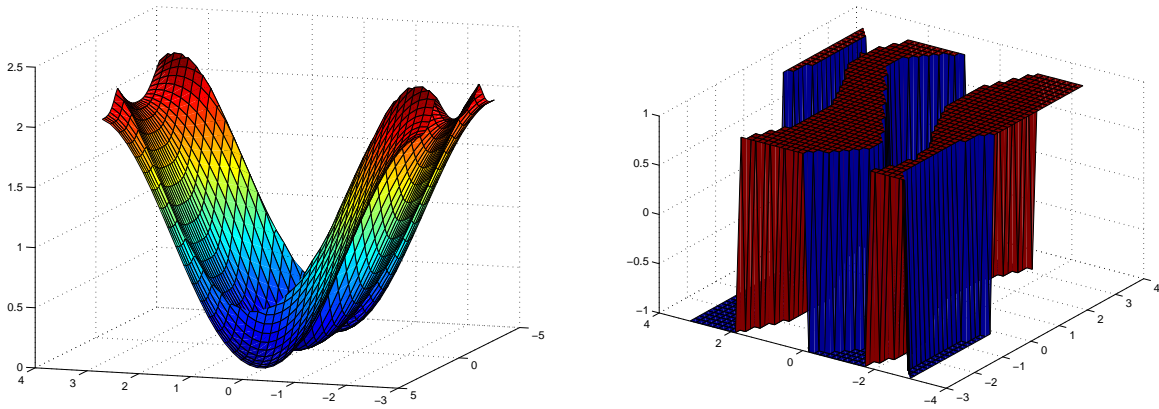

Figure 3.10: Example 3.12. $t = 1$. $CFL = 0.1$. P^2 polynomials on a 40×40 uniform mesh. Penalty constant: $C = 0.25$. Left: the numerical solution; right: $\text{sign}(\varphi_y)$.

Table 3.12: Errors and numerical orders of accuracy for Example 3.13 when using P^2 polynomials and third order Runge-Kutta time discretization on triangular meshes with characteristic length h. Penalty constant $C = 0.25$. Final time $t = 0.5/\pi^2$. $CFL = 0.1$.

h	L^2 error	order	L^2 error	order	L^∞ error	order
1	1.05E-02		1.65E-02		1.48E-01	
1/2	1.59E-03	2.71	2.49E-03	2.73	3.11E-02	2.25
1/4	2.42E-04	2.71	4.02E-04	2.63	6.35E-03	2.29
1/8	3.28E-05	2.89	5.84E-05	2.78	1.03E-03	2.62
1/16	3.96E-06	3.05	7.45E-06	2.97	1.72E-04	2.58
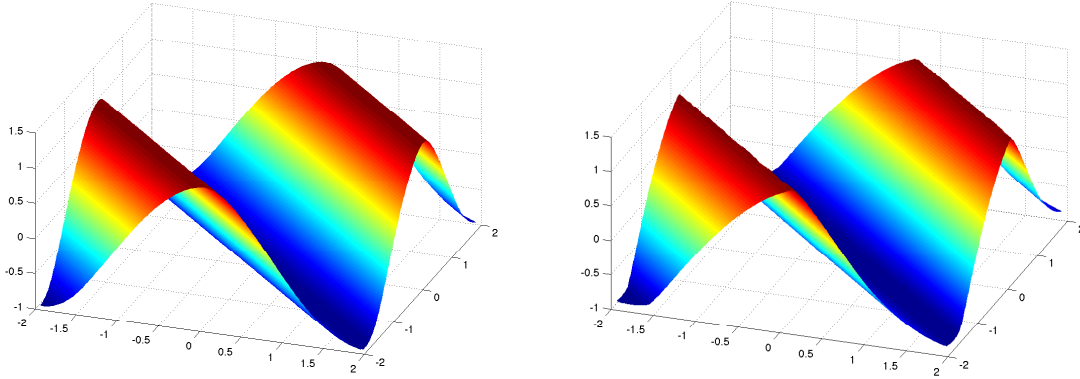
Figure 3.11: Example 3.13. $CFL = 0.1$. P^2 polynomials. Triangular mesh with characteristic length 1/8. 2816 elements. Penalty constant: $C = 0.25$. Left: $t = 0.5/\pi^2$. Right: $t = 1.5/\pi^2$.
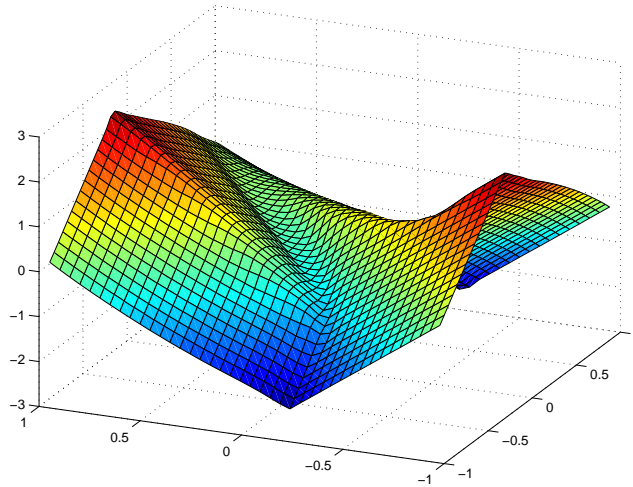

Figure 3.12: Example 3.14. $t = 1$. $CFL = 0.1$. P^2 polynomials on a 41×41 uniform mesh. Penalty constant: $C = 0.25$.

Example 3.15 The problem of a propagating surface

$$\begin{cases} \varphi_t - \sqrt{\varphi_x^2 + \varphi_y^2 + 1} = 0 \\ \varphi(x, y, 0) = 1 - \dfrac{1}{4}(\cos(2\pi x) - 1)(\cos(2\pi y) - 1) \end{cases} \tag{3.30}$$

22

with periodic boundary condition on the domain $[0, 1]^2$. This is a special case of the example used in [19], and is also the two-dimensional Eikonal equation arising from geometric optics [15]. We use an unstructured mesh shown in Figure 3.13 with refinements near the center of the domain where the solution develops singularity. The numerical solutions at different times are displayed in Figure 3.14. Notice that the solution at $t = 0$ is shifted downward by 0.35 to show the detail of the solutions at later times.
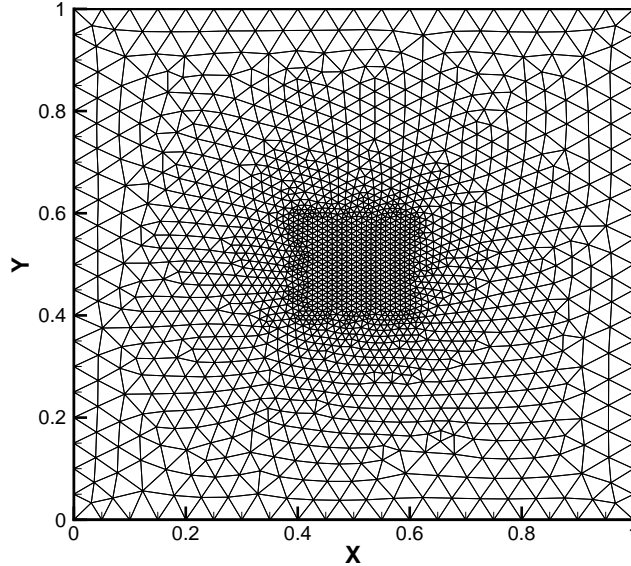
Figure 3.13: Example 3.15. The unstructured mesh used in the computation. Number of elements: 3480.

Example 3.16 The problem of a propagating surface on the unit disk $\{(x, y) : x^2 + y^2 \leq 1\}$

$$\begin{cases} \varphi_t - \sqrt{\varphi_x^2 + \varphi_y^2 + 1} = 0 \\ \varphi(x, y, 0) = -\sin(\dfrac{\pi(x^2 + y^2)}{2}). \end{cases} \tag{3.31}$$

We use an unstructured mesh as depicted in Figure 3.15 with refinements near the origin where solution develops singularity. The numerical solutions at different times are displayed in Figure 3.16. Notice that the solution at $t = 0$ is shifted downward by 0.2 to show the detail of the solutions at later times.

4 Concluding Remarks

In this paper, we propose a new DG method for directly solving the HJ equation. The scheme is direct and robust, and is demonstrated to work on unstructured meshes even with nonconvex Hamiltonians. The theoretical aspects of this method are subjects of future study.
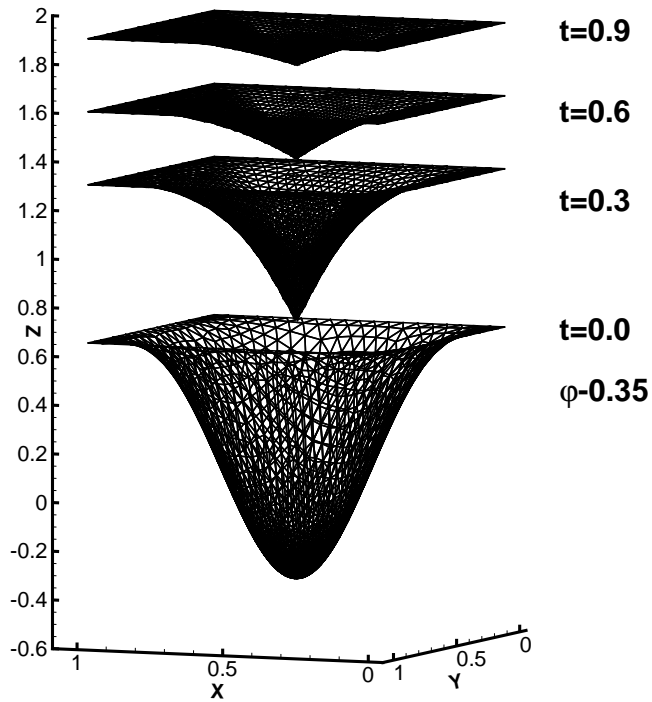
Figure 3.14: Example 3.15. $CFL = 0.1$. P^2 polynomials. Penalty constant: $C = 0.25$. The numerical solution at the indicated times.
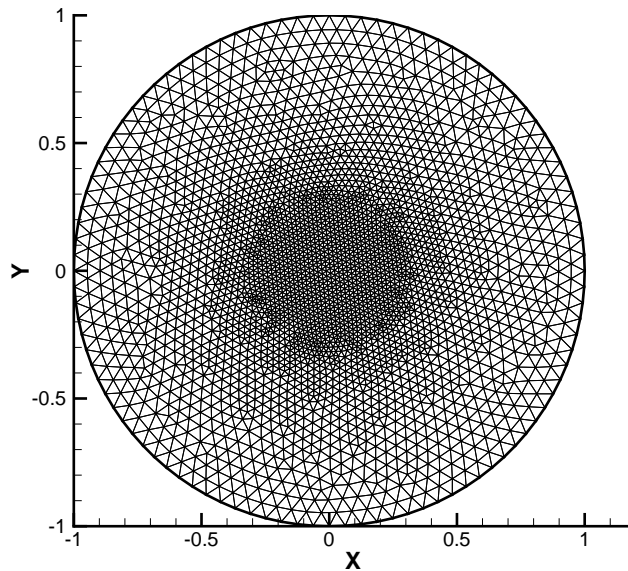

Figure 3.15: Example 3.16. The unstructured mesh used in the computation. Number of elements: 5890.

References

[1] R. Abgrall. Numerical discretization of the first-order Hamilton-Jacobi equation on triangular meshes. *Commun. Pur. Appl. Math.*, 49(12):1339–1373, 1996.
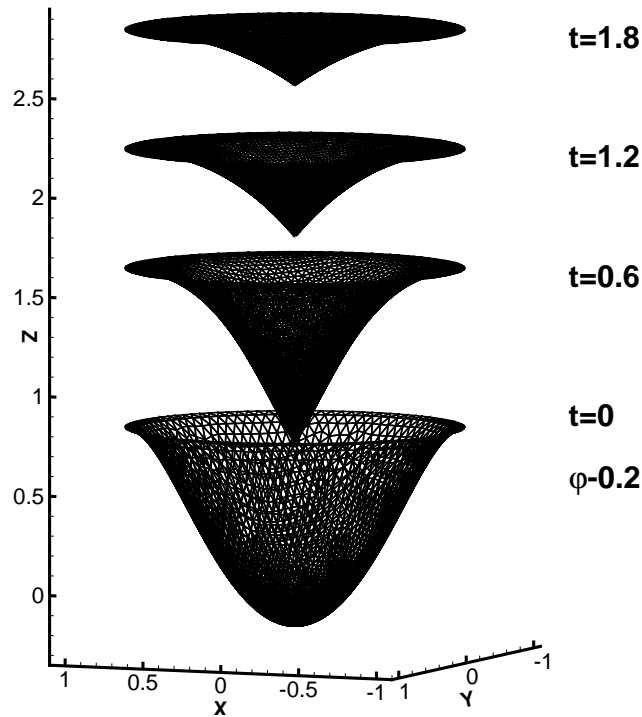
Figure 3.16: Example 3.16. $CFL = 0.1$. P^2 polynomials. Penalty constant: $C = 0.25$. The numerical solution at the indicated times.

[2] O. Bokanowski, Y. Cheng, and C.-W. Shu. A discontinuous Galerkin solver for front propagation with obstacles. *Numer. Math.* to appear.

[3] O. Bokanowski, Y. Cheng, and C.-W. Shu. A discontinuous Galerkin solver for front propagation. *SIAM J. Sci. Comput.*, 33:923–938, 2011.

[4] Y. Chen and B. Cockburn. An adaptive high-order discontinuous Galerkin method with error control for the Hamilton-Jacobi equations. Part I: The one-dimensional steady state case. *J. Comput. Phys.*, 226(1):1027–1058, 2007.

[5] Y. Cheng and C.-W. Shu. A discontinuous Galerkin finite element method for directly solving the Hamilton-Jacobi equations. *J. Comput. Phys.*, 223:398–415, 2007.

[6] B. Cockburn and C.-W. Shu. Runge-Kutta discontinuous Galerkin methods for convection-dominated problems. *J. Sci. Comput.*, 16:173–261, 2001.

[7] M. G. Crandall, L. C. Evans, and P.-L. Lions. Some properties of viscosity solutions of hamilton-jacobi equations. *Trans. Amer. Math. Soc.*, 282(2):487–502, 1984.

[8] M. G. Crandall and P.-L. Lions. Viscosity solutions of Hamilton-Jacobi equations. *Transactions of the American Mathematical Society*, 277:1–42, 1983.

[9] M. G. Crandall and P.-L. Lions. Two approximations of solutions of Hamilton-Jacobi equations. *Math. Comp.*, 43:1–19, 1984.

[10] S. Gottlieb, C.-W. Shu, and E. Tadmor. Strong stability preserving high order time discretization methods. *SIAM Review*, 43:89–112, 2001.

[11] W. Guo, F. Li, and J. Qiu. Local-structure-preserving discontinuous Galerkin methods with Lax-Wendroff type time discretizations for Hamilton-Jacobi equations. *J. Sci. Comput.*, 47(2):239–257, 2011.

[12] A. Harten and J. M. Hyman. Self adjusting grid methods for one-dimensional hyperbolic conservation laws. *J. Comput. Phys.*, 50(2):235–269, 1983.

[13] C. Hu and C.-W. Shu. A discontinuous Galerkin finite element method for Hamilton-Jacobi equations. *SIAM J. Sci. Comput.*, 21:666–690, 1999.

[14] G. Jiang and D. Peng. Weighted ENO schemes for Hamilton-Jacobi equations. *SIAM J. Sci. Comput.*, 21:2126–2143, 1999.

[15] S. Jin and Z. Xin. Numerical passage from systems of conservation laws to Hamilton-Jacobi equations, and relaxation schemes. *SIAM J. Numer. Anal.*, 35(6):2385–2404, 1998.

[16] L. Krivodonova. Limiters for high-order discontinuous Galerkin methods. *J. Comput. Phys.*, 226(1):879–896, 2007.

[17] F. Li and C.-W. Shu. Reinterpretation and simplified implementation of a discontinuous Galerkin method for Hamilton-Jacobi equations. *Appl. Math. Lett.*, 18:1204–1209, 2005.

[18] F. Li and S. Yakovlev. A central discontinuous Galerkin method for Hamilton-Jacobi equations. *J. Sci. Comput.*, 45(1-3):404–428, 2010.

[19] S. Osher and J. A. Sethian. Fronts propagating with curvature-dependent speed: algorithms based on Hamilton-Jacobi formulations. *J. Comput. Phys.*, 79(1):12–49, 1988.

[20] S. Osher and C.-W. Shu. High order essentially non-oscillatory schemes for Hamilton-Jacobi equations. *SIAM J. Numer. Anal.*, 28:907–922, 1991.

[21] C.-W. Shu. High order numerical methods for time dependent Hamilton-Jacobi equations. *Mathematics and Computation in Imaging Science and Information Processing, Lect. Notes Ser. Inst. Math. Sci. Natl. Univ. Singap*, 11:47–91, 2007.

[22] C.-W. Shu. Survey on discontinuous Galerkin methods for Hamilton-Jacobi equations. *Recent Advances in Scientific Computing and Applications*, 586:323, 2013.

[23] C.-W. Shu and S. Osher. Efficient implementation of essentially non-oscillatory shock-capturing schemes. *J. Comput. Phys.*, 77:439–471, 1988.

[24] P. E. Souganidis. Approximation schemes for viscosity solutions of Hamilton-Jacobi equations. *J. Differ. Equations*, 59(1):1–43, 1985.

[25] T. Xiong, C.-W. Shu, and M. Zhang. A priori error estimates for semi-discrete discontinuous Galerkin methods solving nonlinear Hamilton-Jacobi equations with smooth solutions. *Int. J. Numer. Anal. Mod.*, 2013.

[26] J. Yan and S. Osher. A local discontinuous Galerkin method for directly solving Hamilton-Jacobi equations. *J. Comput. Phys.*, 230(1):232–244, 2011.

[27] Y.-T. Zhang and C.-W. Shu. High order WENO schemes for Hamilton-Jacobi equations on triangular meshes. *SIAM J. Sci. Comput.*, 24:1005–1030, 2003.